Letter

Inclusive production of fully charmed tetraquarks at the LHC

Feng Feng,[1,2,*] Yingsheng Huang,[3,4,†] Yu Jia,[2,5,‡] Wen-Long Sang,[6,§] De-Shan Yang,[5,2,‖] and Jia-Yue Zhang[2,5,¶]

[1]*China University of Mining and Technology, Beijing 100083, China*
[2]*Institute of High Energy Physics, Chinese Academy of Sciences, Beijing 100049, China*
[3]*High Energy Physics Division, Argonne National Laboratory, Argonne, Illinois 60439, USA*
[4]*Department of Physics and Astronomy, Northwestern University, Evanston, Illinois 60208, USA*
[5]*School of Physics, University of Chinese Academy of Sciences, Beijing 100049, China*
[6]*School of Physical Science and Technology, Southwest University, Chongqing 400700, People's Republic of China*

(Received 28 April 2023; accepted 4 August 2023; published 5 September 2023)

The $X(6900)$ resonance, originally discovered by the LHCb Collaboration and later confirmed by both the ATLAS and CMS experiments, has sparked broad interest in the fully charmed tetraquark states. Relative to the mass spectra and decay properties of fully heavy tetraquarks, our knowledge on their production mechanism is still rather limited. In this work, we investigate the inclusive production of fully charmed S-wave tetraquarks at the LHC within the nonrelativistic QCD factorization framework. The partonic cross sections are computed at lowest order in α_s and velocity, while the long-distance nonrelativistic QCD matrix elements are estimated from phenomenological potential models. We predict the differential p_T spectra of various fully charmed S-wave tetraquarks at the LHC and compare with the results predicted from the fragmentation mechanism at the large-p_T end.

DOI: 10.1103/PhysRevD.108.L051501

I. INTRODUCTION

In 2020, the LHCb Collaboration reported the unexpected discovery of a new resonance, dubbed $X(6900)$, in the di-J/ψ invariant mass spectrum [1]. Later, in 2022, both the ATLAS and CMS Collaborations [2,3] confirmed the existence of this new particle. $X(6900)$ is widely believed to be a viable candidate for the fully charmed compact tetraquark state [4], though other possibilities have also been explored [5–10]. Since the charm quark is too heavy to be readily knocked out of the vacuum, the dynamic feature of the fully charm tetraquark (hereafter denoted by T_{4c}) is dominated by its leading Fock component $|cc\bar{c}\bar{c}\rangle$ and, thus, free from the contamination by the light constitutes. Analogous to the fact that heavy quarkonia are the simplest hadrons, the fully charmed tetraquarks are the simplest exotic hadrons from a theoretical perspective.

Long before the discovery of $X(6900)$, the existence of possible fully heavy tetraquark states has been explored since the 1970s [11–13]. The mass spectra and decay properties of fully heavy tetraquarks have been investigated from various phenomenological models, including quark potential models [14–26] and QCD sum rules [27–31]. On the other hand, the study of the production mechanism of fully heavy tetraquarks is relatively sparse, which is mainly based on color evaporation model and duality relations [14,32–38]. Inspired by the unexpected discovery of $X(6900)$, recently several groups have attempted to investigate the T_{4c} production in the context of model-independent nonrelativistic QCD (NRQCD) factorization framework [39–43]. Ma and Zhang studied the inclusive production of T_{4c} at the LHC and conducted a numerical study of the dependence of the ratio $\sigma(2^{++})/\sigma(0^{++})$ on p_T [39]. Zhu computed the $gg \to T_{4c}$ channel and predicted the low-p_T spectrum of the T_{4c} at the LHC utilizing Collins-Soper-Sterman resummation [43]. Feng *et al.* explicitly introduced the NRQCD operators relevant to S-wave T_{4c} production and derived the approximate relation between the long-distance NRQCD matrix elements and the tetraquark wave functions at the origin [40]. Feng *et al.* have applied the NRQCD factorization approach to predict the T_{4c} hadroproduction at large p_T

*F.Feng@outlook.com
†yingsheng.huang@northwestern.edu
‡jiay@ihep.ac.cn
§wlsang@swu.edu.cn
‖yangds@ucas.ac.cn
¶zhangjiayue@ihep.ac.cn

via the fragmentation mechanism [40], as well as inclusive and exclusive production of T_{4c} at B factories [41,42].

The goal of this work is to apply the NRQCD factorization approach elaborated in Ref. [40] to investigate the p_T spectrum of the S-wave T_{4c} at the LHC. We focus on the $gg \to T_{4c} + g$ channels and compute the short-distance coefficients at lowest order in α_s and v. We appeal to phenomenological potential models to estimate the nonperturbative NRQCD matrix elements. The numerical studies indicate that there are bright prospects to measure the p_T spectrum of T_{4c}. Since the bulk of cross sections come from the small-p_T regime, where the fragmentation mechanism fails to be applicable, we hope that our fixed-order NRQCD prediction provides more useful guidance for future experimental measurements of the T_{4c} spectrum.

II. NRQCD FACTORIZATION FORMULA FOR T_{4c} HADROPRODUCTION

According to the QCD factorization theorem, the inclusive production rate of the fully charmed tetraquark T_{4c} in hadronic collisions can be expressed as

$$\mathrm{d}\sigma(pp \to T_{4c} + X) = \sum_{i,j=q,g} \int_0^1 dx_1 dx_2 f_{i/p}(x_1, \mu_F) \times f_{j/p}(x_2, \mu_F) \mathrm{d}\hat{\sigma}_{ij \to T_{4c}+X}(x_1 x_2 s, \mu_F), \tag{1}$$

where $f_{i/p}(x, \mu_F)$ denotes the parton distribution function (PDF) of the parton i inside the proton and μ_F represents the factorization scale. $\hat{\sigma}_{ij \to T_{4c}+X}(x_1 x_2 s, \mu_F)$ is the partonic cross section for the $ij \to T_{4c} + X$ channel. If we are interested in T_{4c} production with not overly large p_T, since the gluon density is much more dominant than quark density at small x, it suffices to consider only the gluon-gluon fusion and neglect the $q\bar{q}$ channel.

The partonic cross section $\hat{\sigma}_{ij \to T_{4c}+X}(x_1 x_2 s, \mu_R, \mu_F)$ in Eq. (1) still encapsulates the nonperturbative effects about the formation of the T_{4c}. Since four charm quarks have to be created in relatively short distance to have a non-negligible chance to form T_{4c}, owing to asymptotic freedom, one anticipates that NRQCD factorization can be invoked to further factorize the partonic cross section $\hat{\sigma}_{T_{4c}+X}$ into the product of the perturbatively calculable short-distance coefficients (SDCs) and the nonperturbative long-distance matrix elements (LDMEs):

$$\frac{\mathrm{d}\hat{\sigma}_{T_{4c}+X}}{\mathrm{d}\hat{t}} = \sum_n \frac{F_n(\hat{s}, \hat{t})}{m_c^{14}} (2M_{T_{4c}}) \langle O_n^{T_{4c}} \rangle, \tag{2}$$

where $\mathrm{d}\hat{\sigma}_{T_{4c}+X}$ signifies the partonic cross section for $gg \to T_{4c} + X$. F_n denotes the SDC associated with different color configuration n, and $\langle O_n^{T_{4c}} \rangle$ denotes the vacuum matrix elements of various NRQCD production operators. $\hat{s}$ and $\hat{t}$ are the usual partonic Mandelstam variables. The factor $2M_{T_{4c}}$ is inserted to compensate for the fact that the T_{4c} state is nonrelativistically normalized in the LDMEs.

The main concern of this work is about the S-wave fully charmed tetraquarks, which may carry the J^{PC} quantum number of 0^{++}, 1^{+-}, and 2^{++}. It is convenient to adopt the diquark basis to specify the color configuration. In this context, the color-singlet tetraquark is decomposed into either $\bar{\mathbf{3}} \otimes \mathbf{3}$ or $\mathbf{6} \otimes \bar{\mathbf{6}}$ diquark-antidiquark clusters. The former case corresponds to the spin-1 diquark, while the latter corresponds to the spin-0 diquark.

Specifically speaking, at the lowest order in velocity expansion, Eq. (2) takes the following form:

$$\frac{\mathrm{d}\hat{\sigma}(T_{4c}^{(J)} + X)}{\mathrm{d}\hat{t}} = \frac{2M_{T_{4c}}}{m_c^{14}} \left[F_{3,3}^{(J)} \left\langle O_{3,3}^{(J)} \right\rangle + 2F_{3,6}^{(J)} \left\langle O_{3,6}^{(J)} \right\rangle + F_{6,6}^{(J)} \left\langle O_{6,6}^{(J)} \right\rangle \right], \tag{3}$$

with $J = 0, 1, 2$. $O_{\mathrm{color}}^{(J)}$ denote the NRQCD production operators with different color configuration, which were introduced in Refs. [40–42]:

$$O_{3,3}^{(J)} = \mathcal{O}_{\bar{\mathbf{3}}\otimes\mathbf{3}}^{(J)} \sum_X |T_{4c}^J + X\rangle\langle T_{4c}^J + X| \mathcal{O}_{\bar{\mathbf{3}}\otimes\mathbf{3}}^{(J)\dagger}, \tag{4a}$$

$$O_{6,6}^{(0)} = \mathcal{O}_{\mathbf{6}\otimes\bar{\mathbf{6}}}^{(0)} \sum_X |T_{4c}^0 + X\rangle\langle T_{4c}^0 + X| \mathcal{O}_{\mathbf{6}\otimes\bar{\mathbf{6}}}^{(0)\dagger}, \tag{4b}$$

$$O_{3,6}^{(0)} = \mathcal{O}_{\bar{\mathbf{3}}\otimes\mathbf{3}}^{(0)} \sum_X |T_{4c}^0 + X\rangle\langle T_{4c}^0 + X| \mathcal{O}_{\mathbf{6}\otimes\bar{\mathbf{6}}}^{(0)\dagger}, \tag{4c}$$

with the quartic NRQCD operators $\mathcal{O}_{\bar{\mathbf{3}}\otimes\mathbf{3}}^{(J)}$ and $\mathcal{O}_{\mathbf{6}\otimes\bar{\mathbf{6}}}^{(0)}$ defined by

$$\mathcal{O}_{\bar{\mathbf{3}}\otimes\mathbf{3}}^{(0)} = -\frac{1}{\sqrt{3}} [\psi_a^T (i\sigma^2) \sigma^i \psi_b] [\chi_c^\dagger \sigma^i (i\sigma^2) \chi_d^*] \mathcal{C}_{\bar{\mathbf{3}}\otimes\mathbf{3}}^{ab;cd}, \tag{5a}$$

$$\mathcal{O}_{\bar{\mathbf{3}}\otimes\mathbf{3}}^{i;(1)} = -\frac{i}{\sqrt{2}} \left[\psi_a^T (i\sigma^2) \sigma^j \psi_b\right] \left[\chi_c^\dagger \sigma^k (i\sigma^2) \chi_d^*\right] \epsilon^{ijk} \mathcal{C}_{\bar{\mathbf{3}}\otimes\mathbf{3}}^{ab;cd}, \tag{5b}$$

$$\mathcal{O}_{\bar{\mathbf{3}}\otimes\mathbf{3}}^{ij;(2)} = [\psi_a^T (i\sigma^2) \sigma^m \psi_b] [\chi_c^\dagger \sigma^n (i\sigma^2) \chi_d^*] \Gamma^{ij;mn} \mathcal{C}_{\bar{\mathbf{3}}\otimes\mathbf{3}}^{ab;cd}, \tag{5c}$$

$$\mathcal{O}_{\mathbf{6}\otimes\bar{\mathbf{6}}}^{(0)} = [\psi_a^T (i\sigma^2) \psi_b] [\chi_c^\dagger (i\sigma^2) \chi_d^*] \mathcal{C}_{\mathbf{6}\otimes\bar{\mathbf{6}}}^{ab;cd}. \tag{5d}$$

The color indices a, b, c, and d run from 1 to 3, and the Cartesian indices i, j, and k run from 1 to 3. The rank-4 Lorentz tensor is given by $\Gamma^{kl;mn} \equiv \frac{1}{2}(\delta^{km}\delta^{ln} + \delta^{kn}\delta^{lm} - \frac{2}{3}\delta^{kl}\delta^{mn})$, and the rank-4 color tensors $\mathcal{C}$ are defined as

$$\mathcal{C}^{ab;cd}_{\bar{\mathbf{3}}\otimes\mathbf{3}} \equiv \frac{1}{(\sqrt{2})^2}\epsilon^{abm}\epsilon^{cdn}\frac{\delta^{mn}}{\sqrt{N_c}} = \frac{1}{2\sqrt{3}}(\delta^{ac}\delta^{bd} - \delta^{ad}\delta^{bc}), \tag{6a}$$

$$\mathcal{C}^{ab;cd}_{\mathbf{6}\otimes\bar{\mathbf{6}}} \equiv \frac{1}{2\sqrt{6}}(\delta^{ac}\delta^{bd} + \delta^{ad}\delta^{bc}). \tag{6b}$$

III. DETERMINATION OF SHORT-DISTANCE COEFFICIENTS

We employ the perturbative matching procedure to calculate various SDCs associated with different color channels in Eq. (3). Since the SDCs are insensitive to the long-distance dynamics, one may replace the physical tetraquark states with free four-quark states $|[cc][\bar{c}\bar{c}]\rangle$ in Eq. (3). It is then straightforward to calculate both sides in perturbative QCD and perturbative NRQCD to solve for the SDCs.

We have normalized the NRQCD operators such that all vacuum-to-tetraquark matrix elements of the NRQCD composite operators are equal to 4 (up to a factor of the polarization vector). For the QCD part, we compute the amplitude of $gg \to |[cc][\bar{c}\,\bar{c}]\rangle + g$, employing the covariant color and Lorentz projector method to project out the desired amplitude where the fictitious tetraquark states carry appropriate color, spin, and orbital quantum numbers [40]. We work in Feynman gauge and take $P^2 = M^2_{T_{4c}} \approx 16m_c^2$ for simplicity. We employ our self-written program HepLib [44] alongside FeynArts and FeynCalc [45,46] to generate the Feynman diagrams and square the amplitudes as well as sum over polarizations. There are 642 Feynman diagrams in total, with one typical Feynman diagram shown in Fig. 1. To avoid the occurrence of the ghost contribution, we sum over only two transverse polarizations for the incoming and outgoing gluons upon squaring the amplitude. We have explicitly verified gauge invariance of the squared amplitude.

The complete expressions of the SDCs are too lengthy to be reproduced in the text. For the convenience of the readers, we have attached those expressions in Supplemental Material [47]. Here, we are contented with producing the asymptotic behaviors of various SDCs in the large-p_T limit:

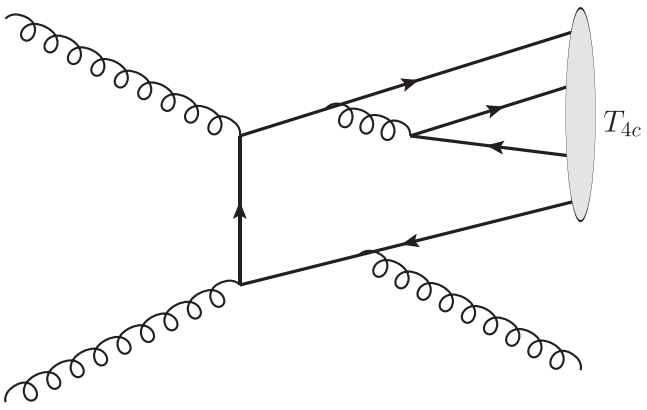

FIG. 1. One typical Feynman diagram for $gg \to T_{4c} + g$.

$$F^{0^{++}}_{3,3} = \frac{2209\pi^4 m_c^6 \alpha_s^5 (\hat{s}\,\hat{t} + \hat{s}^2 + \hat{t}^2)^4}{15552\hat{s}^5(-\hat{t})^3(\hat{s}+\hat{t})^3} + \mathcal{O}\left(\frac{m_c^7}{p_T^7}\right), \tag{7a}$$

$$F^{0^{++}}_{3,6} = \sqrt{6}F^{0^{++}}_{3,3} + \mathcal{O}\left(\frac{m_c^7}{p_T^7}\right), \tag{7b}$$

$$F^{0^{++}}_{6,6} = \frac{2}{3}F^{0^{++}}_{3,3} + \mathcal{O}\left(\frac{m_c^7}{p_T^7}\right), \tag{7c}$$

$$F^{1^{+-}}_{3,3} = \frac{60025\pi^4 m_c^8 \alpha_s^5 (\hat{s}\,\hat{t} + \hat{s}^2 + \hat{t}^2)^2}{34992\hat{s}^4\hat{t}^2(\hat{s}+\hat{t})^2} + \mathcal{O}\left(\frac{m_c^9}{p_T^9}\right), \tag{7d}$$

$$F^{2^{++}}_{3,3} = \frac{17617\pi^4 m_c^6 \alpha_s^5 (\hat{s}\,\hat{t} + \hat{s}^2 + \hat{t}^2)^4}{38880\hat{s}^5(-\hat{t})^3(\hat{s}+\hat{t})^3} + \mathcal{O}\left(\frac{m_c^7}{p_T^7}\right), \tag{7e}$$

with $\hat{s}$ and $\hat{t}$ scaling as $\mathcal{O}(p_T^2)$. Notice that all five SDCs are positive. We also observe that the partonic cross sections for C-even tetraquarks scale as p_T^{-6}, while those for the C-odd state 1^{+-} scale as $\mathcal{O}(p_T^{-8})$. Thus, the production rate of C-odd tetraquark is severely suppressed with respect to the C-even ones due to the extra power of p_T^{-2}. At large p_T, the predicted leading-order (LO) cross sections for the C-even states receive an extra suppression factor of p_T^{-2} with respect to the production rates predicted from the fragmentation mechanism [40], which scale as p_T^{-4}.

IV. PHENOMENOLOGY OF T_{4c} PRODUCTION AT THE LHC

A key ingredient in making concrete predictions is the LDMEs that enter the NRQCD factorization formula (3). These nonperturbative matrix elements can, in principle, be calculated by lattice NRQCD in the future. As a workaround, we appeal to phenomenological approaches to roughly estimate the values of these LDMEs.

After applying the vacuum saturation approximation, one may express the NRQCD LDMEs in terms of the wave functions at the origin of a tetraquark [40–42]:

$$\langle O^{(0)}_{C_1,C_2}\rangle \approx 16\psi^{(0)}_{C_1}(\mathbf{0})\psi^{(0)*}_{C_2}(\mathbf{0}), \tag{8a}$$

$$\langle O^{(1)}_{C_1,C_2}\rangle \approx 48\psi^{(1)}_{C_1}(\mathbf{0})\psi^{(1)*}_{C_2}(\mathbf{0}), \tag{8b}$$

$$\langle O^{(2)}_{C_1,C_2}\rangle \approx 80\psi^{(2)}_{C_1}(\mathbf{0})\psi^{(2)*}_{C_2}(\mathbf{0}), \tag{8c}$$

where $\psi(\mathbf{0})$ denotes the four-body Schrödinger wave function at the origin. The color structure labels C_1 and C_2 can be either 3 or 6, representing the $\bar{\mathbf{3}}\otimes\mathbf{3}$ and the $\mathbf{6}\otimes\bar{\mathbf{6}}$ diquark-antidiquark configuration. In this work, we

TABLE I. Numerical values of the LDMEs estimated from model I and model II.

	LDME	Model I [15]	Model II [16]
0^{++}	$\langle O_{3,3}^{(0)}\rangle$ [GeV^9]	0.0347	0.0187
	$\langle O_{3,6}^{(0)}\rangle$ [GeV^9]	0.0211	−0.0161
	$\langle O_{6,6}^{(0)}\rangle$ [GeV^9]	0.0128	0.0139
1^{+-}	$\langle O_{3,3}^{(1)}\rangle$ [GeV^9]	0.0780	0.0480
2^{++}	$\langle O_{3,3}^{(2)}\rangle$ [GeV^9]	0.072	0.0628

adopt two phenomenological potential models to estimate the wave functions at the origin [15,16]. Both models assume Cornell-type spin-independent potential, incorporate some pieces of spin-dependent potentials, and numerically solve the four-body Schrödinger equation using the Gaussian basis. As a slight difference, model I is based on a nonrelativistic quark potential model, while model II utilizes the relativistic kinetic term. We enumerate the values of the predicted NRQCD LDMEs from both models in Table I. We note that the values of LDMEs have a considerable model dependence, particularly for the 0^{++} channel. Unfortunately, unlike the case from potential NRQCD [48], it lacks a systematic way to estimate the uncertainties of the LDMEs from potential quark models. In this work, we provide the theoretical predictions from the two models, the difference of which is roughly considered as the underlying model uncertainties.

We then apply Eq. (3) in conjunction with Eq. (1) to predict the p_T spectrum of the T_{4c} in pp collision at $\sqrt{s} = 13$ TeV. We set the charm quark mass $m_c = 1.5$ GeV and use $\alpha_s(M_Z) = 0.1180$ [49]. We adopt the CT14lo PDF set [49] and impose a rapidity cut $|y| \leq 5$. We choose the factorization scale $\mu_F = m_T$, with the transverse mass $m_T \equiv \sqrt{M_{T_{4c}}^2 + p_T^2}$. To estimate the uncertainties arising from higher-order QCD corrections, we slide the factorization scale in the range $m_T/2 \leq \mu_F \leq 2m_T$.

The numerical predictions for the p_T spectra of various S-wave T_{4c} states are plotted in Figs. 2 and 3. In Fig. 2, we compare the p_T distributions of different T_{4c} states, taking both potential models as inputs. The lower insets show the ratios of the $\sigma(1^{+-})$ and $\sigma(2^{++})$ states to $\sigma(0^{++})$. We observe that, while the difference between C-even states is minor, the C-odd 1^{+-} state exhibits much more suppressed cross sections with respect to the C-even tetraquarks. This observation corroborates the asymptotic p_T scaling behaviors shown in Eq. (7), where the differential cross section for the 1^{+-} tetraquark is suppressed by a factor of $1/p_T^2$ with respect to those for the C-even tetraquarks.

In Fig. 3, we compare the predictions made from two phenomenological models. Note that the two models, in general, render similar results, except in the case of the 0^{++} tetraquark. It is the interfering term $2F_{3,6}\langle O_{3,6}\rangle$ in Eq. (3) that is responsible for the drastic difference. As shown in Table I, the values of $\langle O_{3,6}\rangle$ in the two models even take different signs. Therefore, the interfering term is constructive in model I and destructive in model II. As a result, the 0^{++} state is suppressed in model II. The impact of the interference is demonstrated in Fig. 4, where we single out the individual contributions from different color configurations in Eq. (3). In model I, the $\bar{\mathbf{3}} \otimes \mathbf{3}$ channel dominates in magnitude, while the other two channels still pose significant positive contributions. It is not the case in model II: The interfering term is negative, and the absolute values of all three color channels are roughly the same.

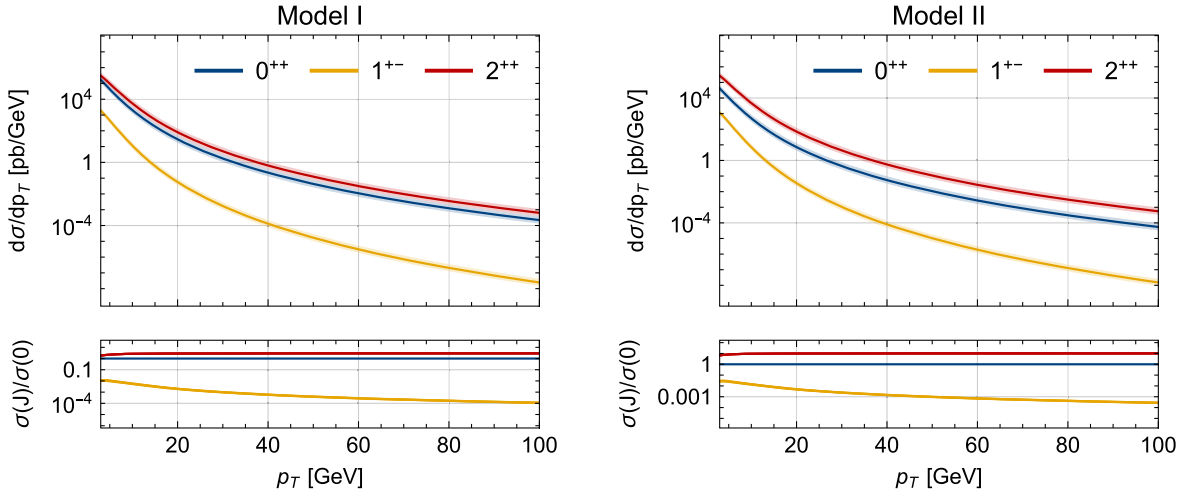

FIG. 2. The p_T spectra of the S-wave T_{4c} at the LHC with $\sqrt{s} = 13$ TeV predicted from two potential models. The left panel represents the predictions made from model I, while the right panel represents the predictions made from model II. The blue, yellow, and red curves represent the differential cross sections for the 0^{++}, 1^{+-}, and 2^{++} tetraquarks, respectively. The lower insets show the ratios of $\sigma(1^{+-})$ and $\sigma(2^{++})$ to $\sigma(0^{++})$.

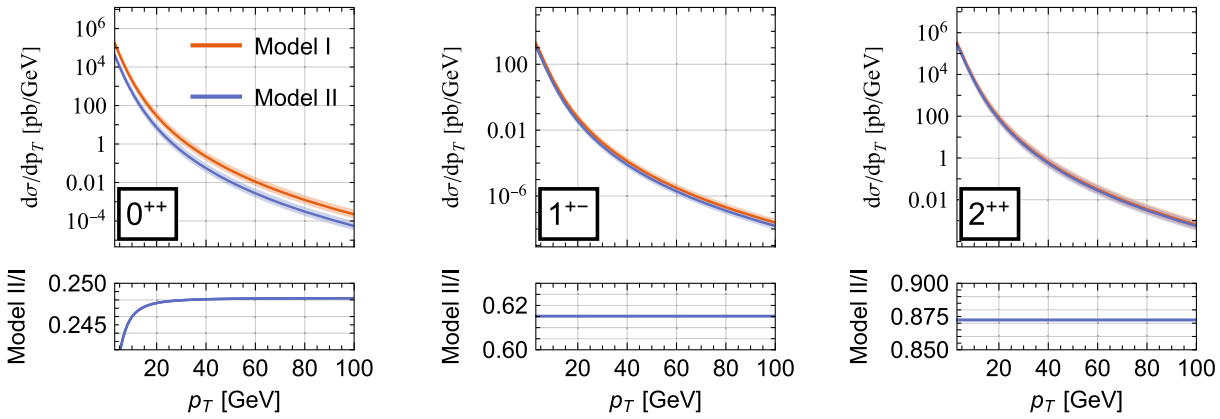

FIG. 3. Comparison of the p_T distributions of the S-wave T_{4c} between two phenomenological potential models. The left, central, and right panels represent the differential cross sections for the 0^{++}, 1^{+-}, and 2^{++} tetraquarks, respectively. The orange (blue) curves represent the predictions made from model I (II). The lower insets show the ratios of the predicted production rates in model II to those in model I.

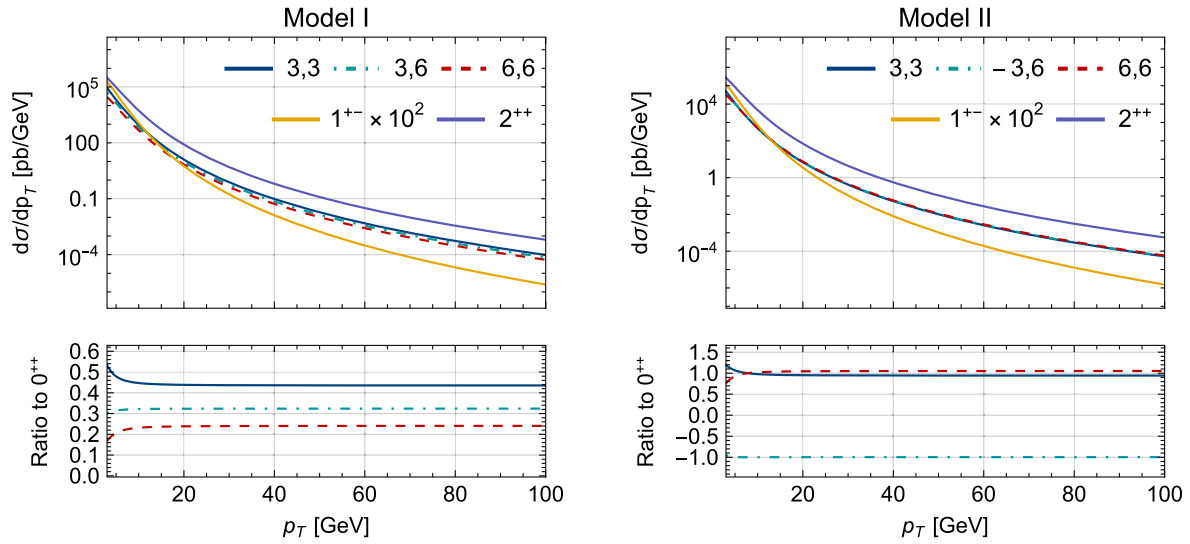

FIG. 4. Comparison of contributions from different color configurations in Eq. (3). The left panel is from model I, and the right panel is for model II. The blue solid, green dash-dotted, and red dashed curves stand for the contributions from the pure color-triplet, interference, and pure color-sextet contributions in $\sigma(0^{++})$, respectively. An additional minus sign is added to the interfering term in model II to make it positive. The lower insets show the ratio of the individual contributions to the full cross section of the 0^{++} tetraquark. We also present the p_T distributions of the 1^{+-} and 2^{++} states for comparison.

In Fig. 5, we also compare our results with the predictions made by the fragmentation mechanism [40]. As indicated in Eq. (7), the fragmentation contribution is enhanced by a factor of p_T^2 relative to our LO NRQCD predictions at large p_T. This expectation is confirmed in Fig. 5, where the fragmentation contributions start to overshoot the LO results when $p_T \sim 20$ GeV.

Finally, in Table II, we present the predicted integrated cross sections for S-wave T_{4c} at $\sqrt{s} = 13$ TeV with a cut $p_T \geq 6$ GeV. Assuming an integrated luminosity of 3000 fb^{-1}, we also estimate the yields of T_{4c} events at the LHC. The yields are roughly 2 orders of magnitude greater than the event yields from fragmentation contributions. This is simply due to the fact that the bulk of the T_{4c} cross sections reside in the low-p_T region.

We note that the T_{4c} cross sections predicted in this work are several orders of magnitude larger than the predictions made in Ref. [43], which range from 10 to 100 fb. Moreover, the ratio of $\sigma(2^{++})$ to $\sigma(0^{++})$ is predicted to be around 2–10 in this work, much smaller than that given in Ref. [43] (about 260) yet relatively closer to the estimation given in Ref. [39] (about 1 and 2).

It is also interesting to compare our predictions for the 1^{+-} T_{4c} events with the measured double J/ψ production

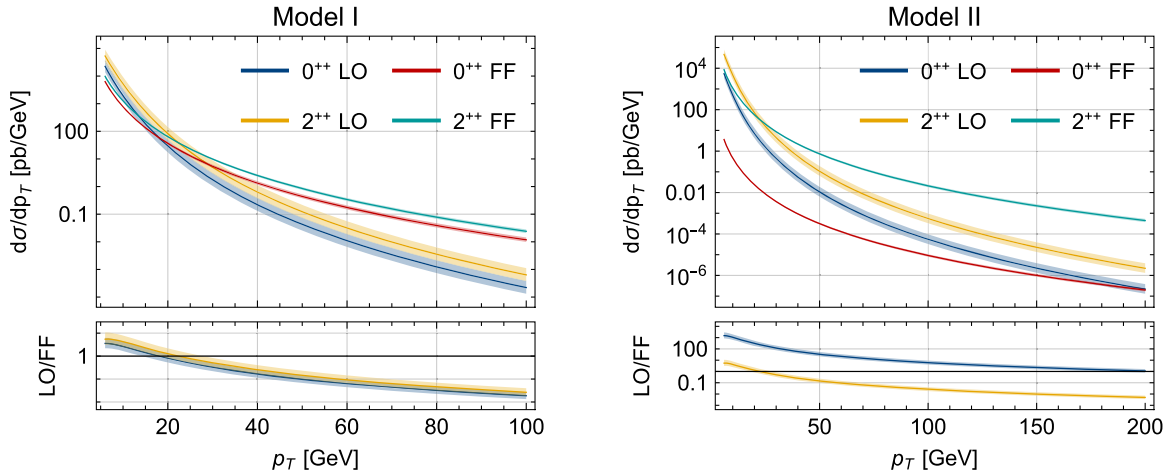

FIG. 5. Comparison of the p_T distributions of the T_{4c} between this work and from the fragmentation mechanism [40]. The left panel is for model I, and the right panel is from model II. The blue and yellow curves represent the LO NRQCD predictions for $\sigma(0^{++})$ and $\sigma(2^{++})$, respectively, while the red and green curves represent the fragmentation contributions to $\sigma(0^{++})$ and $\sigma(2^{++})$, respectively. The lower insets show the ratios of the LO NRQCD predictions to the fragmentation predictions.

rate at ATLAS, which is presumed to arise from double parton scattering [50]. The predicted cross sections of T_{4c} is almost 50 times larger than that for double J/ψ production, which is about 5 pb at 7 TeV.

Exact values of the LDMEs of T_{4b} are absent in the literature. As a very crude estimate, we temporarily assume that T_{4Q} is comprised of a compact diquark-antidiquark cluster, each of which is bound by attractive color Coulomb forces. One then estimates the ratio of the four-body Schrödinger wave functions at the origin for T_{4c} and for T_{4b} through simple dimensional analysis. Hence, we may roughly estimate the LDMEs of the T_{4b} by

$$\begin{aligned}\langle O^{(J)}_{C_1,C_2}\rangle_{T_{4b}} &= \langle O^{(J)}_{C_1,C_2}\rangle_{T_{4c}} \times \frac{\langle O\rangle_{T_{4b},\mathrm{Coulomb}}}{\langle O\rangle_{T_{4c},\mathrm{Coulomb}}} \\ &\approx \langle O^{(J)}_{C_1,C_2}\rangle_{T_{4c}} \times \left(\frac{m_b\alpha_s^b}{m_c\alpha_s^c}\right)^9 \approx 400\times\langle O^{(J)}_{C_1,C_2}\rangle_{T_{4c}},\end{aligned} \tag{9}$$

where α_s^Q represents the strong coupling $\alpha_s(m_Q v_Q)\sim v_Q$, v_Q stands for the typical velocity of the heavy quark Q inside the tetraquark, and the subscript "Coulomb" indicates that the LDME is evaluated using the diquark model with the interquark and interdiquark potentials being Coulombic. It is straightforward to compute the T_{4b} production cross sections. By imposing the same rapidity y cut as T_{4c} and $p_T > 4m_b \approx 20$ GeV, we predict $\sigma = 2$–5, 0.01–0.05, and 4–13 pb for 0^{++}, 1^{+-}, and 2^{++}, respectively.

TABLE II. The integrated production rates for various S-wave T_{4c} states (6 GeV $\le p_T \le$ 100 GeV) and the estimated event yields.

	Model I		Model II	
	σ [nb]	$N_{\mathrm{events}}/10^9$	σ [nb]	$N_{\mathrm{events}}/10^9$
0^{++}	37 ± 26	110 ± 80	9 ± 6	27 ± 19
1^{+-}	0.28 ± 0.16	0.8 ± 0.5	0.17 ± 0.10	0.52 ± 0.29
2^{++}	93 ± 65	280 ± 200	81 ± 57	240 ± 170

V. SUMMARY

In this paper, we predict the p_T spectrum of various S-wave fully charmed tetraquark states within the NRQCD factorization framework, at the lowest order in α_s and velocity. The LDMEs are estimated from two phenomenological potential models, with the aid of vacuum saturation approximation. The yield of the 1^{+-} fully charmed tetraquark is significantly lower than that for the 0^{++} and 2^{++} tetraquarks. Two potential models render quite different predictions for the differential production rates for the 0^{++} tetraquark, signaling the important role played by the interference between the $\bar{\mathbf{3}}\otimes\mathbf{3}$ and $\mathbf{6}\otimes\bar{\mathbf{6}}$ color channels. Both models predict that a tremendous number of T_{4c} events would be produced at the LHC. It is interesting to await future experiments measurements to confront our predictions.

ACKNOWLEDGMENTS

We are grateful to Ming-Sheng Liu and Qi-Fang Lü for providing us with the values of tetraquark wave functions at the origin from their potential models. The work of F. F. is supported by National Natural Science Foundation of China (NNSFC) Grants No. 12275353 and No. 11875318. The work of Y.-S. H. is supported by Department of Energy

Grants No. DE-FG02-91ER40684 and No. DE-AC02-06CH11357. The work of Y. J. and J.-Y. Z. is supported in part by NNSFC Grants No. 11925506 and No. 12070131001 (CRC110 by Deutsche Forschungsgemeinschaft and National Science Foundation of China). The work of W.-L. S. is supported by NNSFC Grant No. 11975187. The work of D.-S. Y. is supported by NNSFC Grant No. 12235008.

[1] R. Aaij *et al.* (LHCb Collaboration), Sci. Bull. **65**, 1983 (2020).
[2] ATLAS Collaboration, Report No. ATLAS-CONF-2022-040.
[3] CMS Collaboration, Report No. CMS-PAS-BPH-21-003.
[4] H. X. Chen, W. Chen, X. Liu, Y. R. Liu, and S. L. Zhu, Rep. Prog. Phys. **86**, 026201 (2023).
[5] J. Z. Wang, D. Y. Chen, X. Liu, and T. Matsuki, Phys. Rev. D **103**, 071503 (2021).
[6] X. K. Dong, V. Baru, F. K. Guo, C. Hanhart, and A. Nefediev, Phys. Rev. Lett. **126**, 132001 (2021); **127**, 119901(E) (2021).
[7] Z. H. Guo and J. A. Oller, Phys. Rev. D **103**, 034024 (2021).
[8] C. Gong, M. C. Du, Q. Zhao, X. H. Zhong, and B. Zhou, Phys. Lett. B **824**, 136794 (2022).
[9] Z. H. Guo and J. A. Oller, Phys. Rev. D **103**, 034024 (2021).
[10] Z. R. Liang, X. Y. Wu, and D. L. Yao, Phys. Rev. D **104**, 034034 (2021).
[11] Y. Iwasaki, Phys. Rev. Lett. **36**, 1266 (1976).
[12] K. T. Chao, Z. Phys. C **7**, 317 (1981).
[13] J. P. Ader, J. M. Richard, and P. Taxil, Phys. Rev. D **25**, 2370 (1982).
[14] C. Becchi, J. Ferretti, A. Giachino, L. Maiani, and E. Santopinto, Phys. Lett. B **811**, 135952 (2020).
[15] Q. F. Lü, D. Y. Chen, and Y. B. Dong, Eur. Phys. J. C **80**, 871 (2020).
[16] M. S. liu, F. X. Liu, X. H. Zhong, and Q. Zhao, arXiv:2006.11952.
[17] M. Karliner and J. L. Rosner, Phys. Rev. D **102**, 114039 (2020).
[18] J. Zhao, S. Shi, and P. Zhuang, Phys. Rev. D **102**, 114001 (2020).
[19] Z. Zhao, K. Xu, A. Kaewsnod, X. Liu, A. Limphirat, and Y. Yan, Phys. Rev. D **103**, 116027 (2021).
[20] J. F. Giron and R. F. Lebed, Phys. Rev. D **102**, 074003 (2020).
[21] H. W. Ke, X. Han, X. H. Liu, and Y. L. Shi, Eur. Phys. J. C **81**, 427 (2021).
[22] M. C. Gordillo, F. De Soto, and J. Segovia, Phys. Rev. D **102**, 114007 (2020).
[23] G. Yang, J. Ping, L. He, and Q. Wang, arXiv:2006.13756.
[24] X. Jin, Y. Xue, H. Huang, and J. Ping, Eur. Phys. J. C **80**, 1083 (2020).
[25] H. Mutuk, Phys. Lett. B **834**, 137404 (2022).
[26] G. J. Wang, Q. Meng, and M. Oka, Phys. Rev. D **106**, 096005 (2022).
[27] H. X. Chen, W. Chen, X. Liu, and S. L. Zhu, Sci. Bull. **65**, 1994 (2020).
[28] Z. G. Wang, Chin. Phys. C **44**, 113106 (2020).
[29] B. C. Yang, L. Tang, and C. F. Qiao, Eur. Phys. J. C **81**, 324 (2021).
[30] B. D. Wan and C. F. Qiao, Phys. Lett. B **817**, 136339 (2021).
[31] J. R. Zhang, Phys. Rev. D **103**, 014018 (2021).
[32] M. Karliner, S. Nussinov, and J. L. Rosner, Phys. Rev. D **95**, 034011 (2017).
[33] A. V. Berezhnoy, A. K. Likhoded, A. V. Luchinsky, and A. A. Novoselov, Phys. Rev. D **84**, 094023 (2011).
[34] A. V. Berezhnoy, A. V. Luchinsky, and A. A. Novoselov, Phys. Rev. D **86**, 034004 (2012).
[35] C. Becchi, A. Giachino, L. Maiani, and E. Santopinto, Phys. Lett. B **806**, 135495 (2020).
[36] R. Maciuła, W. Schäfer, and A. Szczurek, Phys. Lett. B **812**, 136010 (2021).
[37] F. Carvalho, E. R. Cazaroto, V. P. Gonçalves, and F. S. Navarra, Phys. Rev. D **93**, 034004 (2016).
[38] V. P. Gonçalves and B. D. Moreira, Phys. Lett. B **816**, 136249 (2021).
[39] Y. Q. Ma and H. F. Zhang, arXiv:2009.08376.
[40] F. Feng, Y. Huang, Y. Jia, W. L. Sang, X. Xiong, and J. Y. Zhang, Phys. Rev. D **106**, 114029 (2022).
[41] F. Feng, Y. Huang, Y. Jia, W. L. Sang, and J. Y. Zhang, Phys. Lett. B **818**, 136368 (2021).
[42] Y. Huang, F. Feng, Y. Jia, W. L. Sang, D. S. Yang, and J. Y. Zhang, Chin. Phys. C **45**, 093101 (2021).
[43] R. Zhu, Nucl. Phys. **B966**, 115393 (2021).
[44] F. Feng, Y. F. Xie, Q. C. Zhou, and S. R. Tang, Comput. Phys. Commun. **265**, 107982 (2021).
[45] T. Hahn, Comput. Phys. Commun. **140**, 418 (2001).
[46] V. Shtabovenko, R. Mertig, and F. Orellana, Comput. Phys. Commun. **207**, 432 (2016).
[47] See Supplemental Material at http://link.aps.org/supplemental/10.1103/PhysRevD.108.L051501 for the complete expressions of the SDCs.
[48] B. Assi and M. L. Wagman, arXiv:2305.01685.
[49] S. Dulat, T. J. Hou, J. Gao, M. Guzzi, J. Huston, P. Nadolsky, J. Pumplin, C. Schmidt, D. Stump, and C. P. Yuan, Phys. Rev. D **93**, 033006 (2016).
[50] J. P. Lansberg and H. S. Shao, Phys. Lett. B **751**, 479 (2015).